



HAL
open science

Electrical control of the elastic wave propagation in a piezoelectric plate: reduction of the crosstalk in a multi-element ultrasonic transducer

Linyu Fei, Lionel Haumesser, Louis-Pascal Tran-Huu-Hue

► To cite this version:

Linyu Fei, Lionel Haumesser, Louis-Pascal Tran-Huu-Hue. Electrical control of the elastic wave propagation in a piezoelectric plate: reduction of the crosstalk in a multi-element ultrasonic transducer. Forum Acusticum, Dec 2020, Lyon, France. pp.2853-2856, 10.48465/fa.2020.0676 . hal-03240295

HAL Id: hal-03240295

<https://hal.science/hal-03240295>

Submitted on 30 May 2021

HAL is a multi-disciplinary open access archive for the deposit and dissemination of scientific research documents, whether they are published or not. The documents may come from teaching and research institutions in France or abroad, or from public or private research centers.

L'archive ouverte pluridisciplinaire **HAL**, est destinée au dépôt et à la diffusion de documents scientifiques de niveau recherche, publiés ou non, émanant des établissements d'enseignement et de recherche français ou étrangers, des laboratoires publics ou privés.

Electric control of the elastic wave propagation in a piezoelectric plate: reduction of the crosstalk in a multi-element ultrasonic transducer

L. Fei¹

L. Haumesser¹

L.-P. Tran-Huu-Hué¹

¹GREMAN, Université de Tours, INSA Centre Val de Loire, 3 rue de la Chocolaterie, 41000 Blois, France
liny.fe@univ-tours.fr

ABSTRACT

The cross couplings in a multi-element ultrasonic transducer create perturbations in its radiation, affecting image quality. This work proposes to use a passive electrical decoupling to reduce the crosstalk phenomenon. A homogeneous piezoelectric plate, covered on one side by a 1D periodic arrangement of thin metallic electrodes and on the other side by a full metallic electrode, is considered. Under electric boundary conditions applied to the periodic electrodes, band gaps can be created at the edge and in the first Brillouin zone. In that way the radiation pattern at the anti-resonance frequency of the first piezoelectric thickness mode can be closer to that of a piston mode. Finite element analysis and experimental measurements show the advent of band gaps in the dispersion curves, which limits the inter-element coupling and thus the parasitic signals in the radiation pattern.

1. INTRODUCTION

Multi-element piezoelectric ultrasonic transducers are widely used in medical or industrial field. However, the crosstalk between the elements is not negligible, which creates disturbances in the radiation and masks the sharp details in the image. The crosstalk phenomenon increases the number of vibrating elements by comparison to the number of electrically excited elements, and produces spurious guided modes. Solutions have been proposed to reduce this drawback. For example, a passive mechanical decoupling between the elements can be achieved by varying the depth of the periodic cut of the piezoelectric ceramics. In addition, an active electrical decoupling procedure has been proposed, in applying to the other elements, except to the active one, a suitable electric voltage [1].

For purpose of cancelling the crosstalk, that is, to make that the electrically excited element vibrates locally and that the radiation pattern is as wide as possible, the solution should keep the thickness mode of the piezoelectric plate and cancel the guided waves in the plate at the same time.

In this paper, we will present the influence of using a passive electrical decoupling, by applying open, short, or mixed open-short conditions to the electrodes of an electroactive phononic crystal. Under certain electric boundary conditions, band gaps can be created at the edge and in the first Brillouin zone. Then, we show that the radiation pattern at the anti-resonance frequency of the first piezoelectric thickness mode can be closer to that of a piston mode.

The paper is organized as follow. First (Sec. 2), the electrical properties of a fully electroded piezoelectric plate and the characteristics of guided waves in this plate but with the periodic set of electrodes on one side, are shown. Its electric impedance shows the anti-resonance frequency of the first thickness mode and the dispersion curves indicate the standing and propagating waves in the plate. Then in Sec. 3, the vibrations of the piezoelectric phononic plate with different electric boundary conditions and their radiation patterns are presented and analyzed. Next, some simulation results are compared to the experimental ones (Sec. 4). Finally, Sec. 5 is the conclusion.

2. PIEZOELECTRIC PLATE WITH PERIODIC ELECTRODES ON ONE SIDE

The system studied in this paper is a one-dimensional piezoelectric Pz26 homogeneous plate polarized along the thickness and covered by a periodic array of conductive electrodes on one side and a full single electrode connected to the ground on the other side, as shown in Fig. 1(a). The electrodes on both sides are considered as perfectly conductive surfaces whose thickness is neglected by comparison to thickness. Plate lateral dimensions (80 mm * 80 mm) are large in comparison to the plate thickness $e = 2.236$ mm. The forty multiple silver electrodes on one side are 1.9 mm in width. The spacing between two neighbouring electrodes is 0.1 mm. On each rectangular electrode, a welded wire is used to apply electric boundary conditions. For 2D finite element calculations (COMSOL Multiphysics), we adopt the same characters in order to depict a unit cell of the piezoelectric sample in Fig. 1(b). The width of the unit cell is 2 mm. On both sides, the periodic Floquet (FP) conditions are applied [2-3] for the mechanical displacements and the electric potentials. The anti-resonance frequency of the first thickness mode of the piezoelectric plate f_a is calculated numerically at 1.032 MHz, which fits the theoretical value that is obtained according to the following equation (Eqn. (1)),

$$f_a = \frac{1}{2e} \sqrt{\frac{C_{33}^D}{\rho}} \quad (1.)$$

where e and ρ are the thickness and the density of the plate, respectively, and C_{33}^D is the elastic coefficient along the axis according to the thickness.

Dispersion curves are then obtained from the simulation using the unit cell model, in the first Brillouin zone (see Fig. 2). Frequencies of the propagating waves are deduced for the real part of the wavenumber for floating potential (open-circuit). Moreover, dispersion curves for the short-circuit (SC) electric boundary condition, i.e. grounded electric condition for all electrodes, are superimposed. In order to indicate the anti-resonance frequency of the first thickness mode of the piezoelectric plate, the curve of the electrical impedance is also shown in Fig. 2.

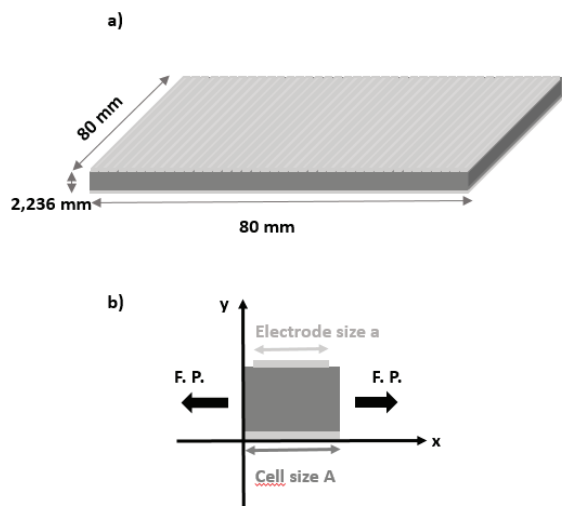


Figure 1. (a) Schematic representation of the phononic piezoelectric plate. (b) Unit cell of the piezoelectric sample.

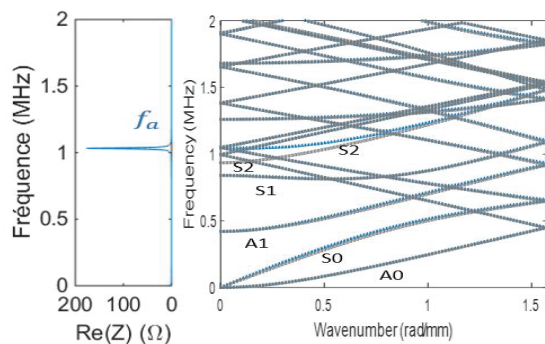


Figure 2. (a) Electric impedance of the plate (b) Dispersion curves of the infinite phononic piezoelectric plate with electrodes having floating potential (blue line) or in short-circuit electric condition (grey line) on one side. A full electrode is connected to the ground on the other side.

It is observed that the dispersion of the different propagation modes are only slightly modified, apart from that of the mode S2 (see Fig. 2). The SC boundary condition shift down the S2 mode and the anti-resonance frequency of the thickness mode is observed at 0.94 MHz. It is expected that this modification interferes with the vibration at the anti-resonance frequency and promotes the localization of the vibration. Thus, we will analyze the vibration and wave radiation of the plate in relation to this observation.

3. NUMERICAL RESULTS FOR VIBRATION AND WAVE RADIATION

The crosstalk in the piezoelectric plate is investigated. For purpose of analysis, the vibrations (i.e. the normal displacements) and the radiation diagrams from the plate are presented. Numerical finite element simulations are made from a 2D model of the piezoelectric plate with forty identical electrodes periodically spaced on one side and on the other side full electrode connected to the ground.

3.1 Normal displacements along the piezoelectric plate

A 10 volts excitation is applied at the 20th electrode. Two situations are compared: open-circuit (OC) or short-circuit (SC), for all sectors except the 20th. Amplitudes of the normal displacements are collected at the grounded electrode side of the plate (Fig. 3).

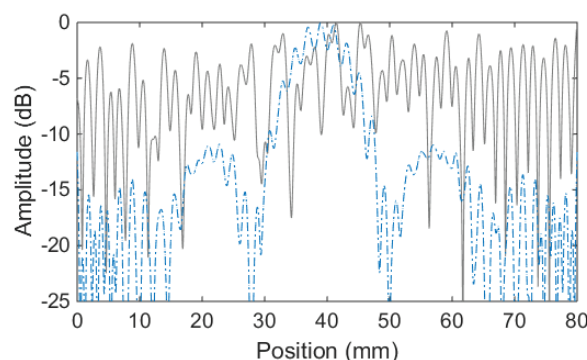


Figure 3. Displacements of the finite phononic piezoelectric plate with electrodes having floating potential (blue dotted line) or short-circuit (grounded) condition (solid grey line).

According to the normal displacement pattern for OC boundary condition, it is observed that the amplitudes of the eleven elements in the middle of the plate are less than -10 dB below the level of the excited element. Therefore, the five elements on both sides of the excited element have a significant contribution to crosstalk. On the other hand, for the SC boundary condition, the vibration amplitude difference between the elements is highly variable and up to -15 dB for the 11 elements in the center, and sharply varying versus position. The radiation diagrams are presented in the next section to observe the effect of this change according to the electric boundary conditions.

3.2 Radiation diagrams and effective parameters

In this section, we present the radiation diagrams obtained from the normal displacements on the grounded electrode side of the phononic piezoelectric plate in OC and SC boundary conditions (see Fig. 4). In order to calculate the radiation diagrams, the Rayleigh formula is considered. The perpendicular axis to the plate is defined at 0 degree. Due to the even number of elements, the diagram is not fully symmetric. A quarter of space from 0 degree to 90 degrees is taken for the comparison. In Fig.

4, the blue line represents the diagram using the OC condition and the red line shows the SC condition diagram, the later being graduated with negative angles.

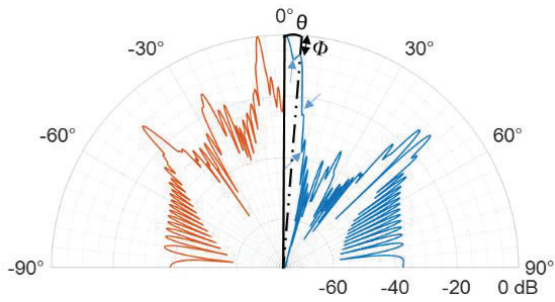


Figure 4. The radiation diagrams of the plate for SC condition (red line) and reference pattern for OC condition (blue line).

In order to analyze the radiation diagrams, the angular directivity formula for N sources is used:

$$H(\theta) = \left| \frac{\sin \frac{\pi L \sin \theta}{\lambda}}{\frac{\pi L \sin \theta}{\lambda}} \right| \left| \frac{\sin \frac{N \pi d \sin \theta}{\lambda}}{\frac{N \pi d \sin \theta}{\lambda}} \right| \quad (2.)$$

where L and d represent the width of each source and the network pitch, respectively.

According to Eqn. (2), an effective width $D = N * d$ is defined, which is equivalent to the width of the vibrating sectors that cause the crosstalk in the plate. To obtain it, the average of the angle deviation between the first five dips, indicated by the blue arrows in Fig. 4 is calculated. The mean value is used in the first term of Eqn. (2) to obtain the effective width value, which is 22 mm for the OC boundary condition (see Tab. 1).

Further, a squint angle θ and the difference in pressure levels Φ in dB are defined (see Fig.4), which are equivalent to the angle of the maximum of the nearest lobe from 0 degree, and the difference between the pressure level at 0 degree and that of the squint angle, respectively. The squint angle in OC condition is 4 degrees and the difference in pressure levels is 7 dB, which are considered as the reference values in this study (blue line in Figs. 4-6). Following the same calculation method, the effective width for the SC boundary condition is equal to 11.9 mm. Hence, the effective width is halved when switching from OC to SC boundary conditions. Moreover, the squint angle is 7 degrees with a difference in pressure levels of -20 dB, which shows a decreased directivity (see Tab. 1). Note that the negative value (-20 dB) is due to the low pressure level at 0 degree.

In the following, two other set of electric boundary conditions are investigated with the 20th excited element. For the one all elements are in OC condition except for the 17th and 23rd sectors which are grounded (SC condition, see Fig. 5(a)). For the other, in a similar way, only the 19th and 21st sectors are grounded (see Fig. 5(b)).

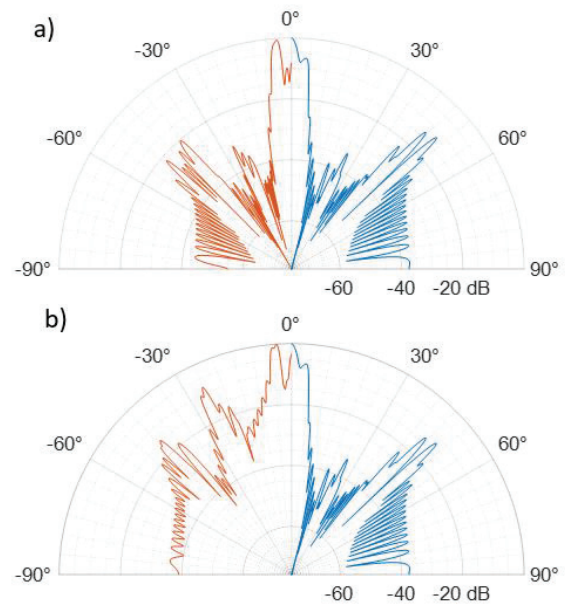


Figure 5. (a) The radiation diagrams of the plate with the SC at the 17th and 23rd sectors only (red line) and reference pattern for OC at all sectors (blue line) (b) Same for the SC at the 19th and 21st sectors only (red line) and reference pattern for OC at all sectors CO (blue line).

Then in order to consider the effect of the new set of boundary conditions on the radiation pattern, the previous parameters are calculated and gathered in Tab. 1.

Boundary condition	OC (ref)	SC	SC at 17 th and 23 rd	SC at 19 th and 21 st
D (mm)	22	11.9	15.2	14.2
θ (°)	4	7	4	4
Φ (dB)	7	-20	-10	-4

Table 1. Effective width, squint angle and difference in pressure levels from radiation patterns for the electric boundary conditions: OC, SC, the SC at 17th and 23rd sectors and the SC at 19th and 21st sectors.

The results for the new sets of boundary conditions yield effective widths equal to 15.2 mm and 14.2 mm, which are intermediate by comparison to OC and SC configurations. In addition, squint angles are found to be of the order to that of the reference configuration, which is not suitable for imaging purpose.

4. EXPERIMENTAL RESULTS

The validation of the results by the experiments is shown in this section for the OC electric boundary condition. A waveform generator is used to deliver a 10 volts electrical tone burst of 1 period centered at the frequency of 1 MHz. The excitation is applied to the 20th sector of the plate. Normal displacements are collected versus time all along the plate. Signals are windowed, which corresponds to a single crossing of the plate. A 2D fast Fourier is performed to obtain the dispersion curves.

The experimental dispersion curves are shown in Fig. 6(a), where we can observe the band gaps created by the periodicity of the electrodes on the plate, at many frequencies and for many modes. For instance, the first gap for the S0 mode is observed around 700 kHz at the edge of the first Brillouin zone, as observed in from Fig 2b. Further, the anti-resonance frequency f_a is 1.030 MHz, which corresponds to the simulated value 1.032 MHz.

From the experimental radiation diagram without time windowing (see Fig. 6(b)), we recover the effective width of 22 mm. Thus, the crosstalk effect in the plate is correctly predicted by the simulation. Nevertheless, it should be noted that between 10 degrees and 40 degrees, the level of experimental radiation is roughly 20 dB higher than that obtained from numerical simulation, which cannot be explained by noise effect in a particular angular range. Further, the squint angle is 5 degrees and the pressure level difference is 9 dB for measurements, which shows reasonable agreement with simulation results.

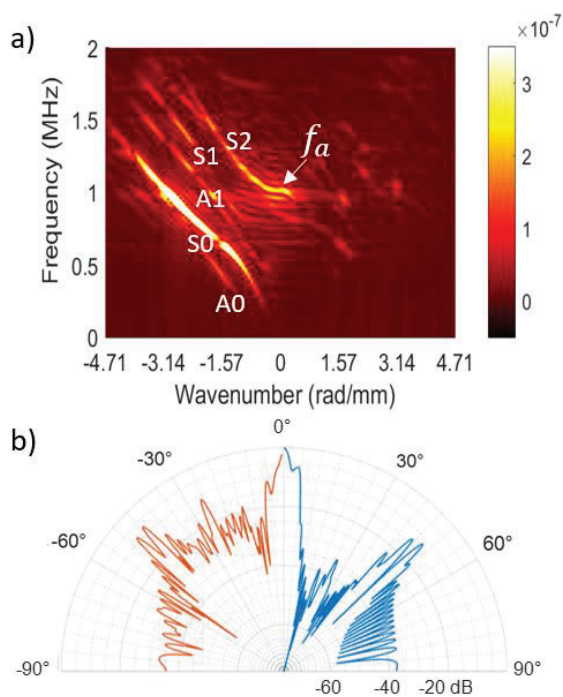


Figure 6. (a) Experimental dispersion curves in OC condition (b) Simulated (blue line) and experimental (red line) radiation patterns, both in OC boundary condition.

5. CONCLUSION

In this work, the effect of various electric boundary conditions on the crosstalk between the elements of an ultrasonic transducer is investigated. Among the tested configurations, the study show that grounding all the elements apart from the excited one reduces the crosstalk effect and changes significantly the radiated pressure field at the anti-resonance frequency of the transducer. In perspective, other possibilities will be trying to create a band gap at the anti-resonance frequency as well to further reduce the crosstalk.

6. REFERENCES

- [1] A. Bybi, C. Granger, S. Grondel, A. Hladkyhennion, and J. Assaad, "Electrical method for crosstalk cancellation in transducer arrays," *NDT & E International*, Vol. 62, pp. 115-121, 2014.
- [2] N. Kherraz, L. Haumesser, F. Levassort, P. Benard, B. Morvan, "Controlling Bragg gaps induced by electric boundary conditions in phononic piezoelectric plates," *Applied Physics Letters*, Vol. 108, No 9, p. 093503, 2016.
- [3] C. Hakoda, J. Rose, P. Shokouhi, C. Lissenden, "Using Floquet Periodicity to Easily Calculate Dispersion Curves and Wave Structures of Homogeneous Waveguides," *AIP Conference Proceedings*. AIP Publishing LLC, p. 020016, 2018.